DOI: 10.1002/cphc.201000576

Rotationally Resolved Electronic Spectroscopy of 1,4-Benzodioxan: The Anomeric Effect in the Ground and Electronically Excited State

Thi Bao Chau Vu,[a] Christian Brand,[a] W. Leo Meerts,[b] and Michael Schmitt*[a]

We measured the rotationally resolved electronic spectra of the origin and of three vibronic bands of 1,4-benzodioxan. From comparison to various ab-initio-calculated structures of 1,4-benzodioxan, the twisted C_2 symmetric 1,4-benzodioxan was shown to be responsible for all the observed spectral features. We analyzed the inertial defects in both electronic states as sensitive indicators of the non-planarity of the system. The molecule was found to be more planar in the electronic ground state than in the electronically excited singlet state. This effect can be traced back to an increased puckering of the dioxan ring, which also comprises the oxygen atoms, in the excited state. This observation is discussed in terms of natural bond orbitals.

1. Introduction

1,4-Benzodioxan (BZD) is a flexible molecule, which is formally derived from *ortho*-di-substituted benzenes, the *ortho* positions being bridged by an $-O-(CH_2)_2-O-$ group. Benzene-fused oxygen-containing compounds are of considerable interest as biomolecular building blocks. Most of what we currently know about structure and large-amplitude motions of BZD comes from the groups of Hollas/Gordon[1–4] and Laane.[5–7]

There is a vast literature on the importance of the anomeric effect for the stabilization of the puckered forms of 1,3-dioxole or 1,3-benzodioxole.[8–10] In these molecules the $n_p \rightarrow \sigma^*_{CO}$ interaction involving the nonbonding lone pair with *p*-character at one oxygen atom and the antibonding σ^*_{CO} orbital of the adjacent CO bond have been shown to contribute most of the stabilization energy of the puckered form.[8] A smaller but hitherto important stabilizing contribution comes from the $n_p \rightarrow \sigma^*_{CH}$ interaction with the antibonding CH orbital.[9,10] In the 1,4-benzodioxan molecule chosen herein, no adjacent CO bond exists; thus, the most important stabilizing contribution in 1,3-benzodioxole is impossible here. Instead, it is the $n_p \rightarrow \sigma^*_{CH}$ interaction which stabilizes the puckered form. This hypothesis can be tested by comparing the extent of the anomeric effect in the ground and electronically excited states. If the electron density is shifted from the oxygen lone pair into the aromatic ring upon electronic excitation, the anomeric effect due to the $n_p \rightarrow \sigma^*_{CH}$ interaction will decrease in the excited state. This effect can be measured via the amount of non-planarity of BZD in both electronic states.

Gordon and Hollas measured the rotational band contour of the 281 nm $\pi\pi^*$ band system of BZD.[1] From symmetry considerations, they determined this system to be due to a A←A transition, as expected for *o*-disubstituted benzenes with C_2 symmetry. From a small inertial defect they deduced a twisted conformation in both electronic states, and the electronic origin ν_0 was determined to be at 35562.48 cm^{-1}. The same group presented single vibronic level fluorescence (SVLF) spectra of various in-plane and out-of-plane bands.[2] Many modes show a strong Duschinsky effect. Using single vibronic level fluorescence and fluorescence excitation (FE) spectroscopy, the modes with the strongest Duschinsky effect were identified as the bending modes ν_{48} and ν_{47}, the latter being also very anharmonic.[3] A very thorough study was performed by Gordon and Hollas, in which a combination of fluorescence excitation and single vibronic level fluorescence was utilized to assign the ground- and excited-state fundamentals of BZD.[4]

Choo et al. made an assignment of the vibrational spectrum of BZD on the basis of density functional theory using Becke's three-parameter hybrid (B3LYP) method.[11] They calculated the energy difference of twisted and bent structures to be 7.5 kcal $mole^{-1}$, the latter being a transition state for the interconversion of two twisted forms.

FE and SVLF spectra for several vibronic states were recorded and analyzed by Yang et al.[5] They calculated a barrier to planarity for the twisted structure at the MP2 level of 4095 cm^{-1}. The experimentally determined frequencies of the ring-twisting states were used for a two-dimensional fit of the barrier, including the bending modes. In this model, barriers for the S_0 state of 3906 cm^{-1} and for the S_1 state of 1744 cm^{-1} were obtained. The structures and frequencies for the two lowest singlet states and the lowest triplet state were reported from a density functional analysis by Yang et al.[6]

[a] *T. B. Chau Vu, C. Brand, Dr. habil. M. Schmitt*
Heinrich-Heine-Universität, Institut für Physikalische Chemie I
40225 Düsseldorf (Germany)
Fax: (+49) 211-81-15195
E-mail: mschmitt@uni-duesseldorf.de

[b] *Prof. Dr. W. L. Meerts*
Radboud University, Institute for Molecules and Materials
Heyendaalseweg 135, NL-6525 AJ Nijmegen (The Netherlands)

Supporting information for this article is available on the WWW under http://dx.doi.org/10.1002/cphc.201000576.

2. Theory

2.1. Ab initio Calculations

Structure optimizations were performed employing the correlation-consistent basis sets of valence triple zeta quality of Dunning (cc-pVTZ) from the TURBOMOLE library.[12,13] The equilibrium geometries of the electronic ground and the lowest excited singlet states were optimized using the approximate coupled cluster singles and doubles model (CC2) employing the resolution-of-the-identity approximation (RI).[14–16]

Ground- and excited-state energies, dipole moments, and transition dipole moments were calculated using the combined density functional theory multi-reference configuration interaction (DFT/MRCI) method[17] with the same basis sets as that used for the structure optimizations. The configuration state functions (CSFs) in the MRCI expansion are constructed from Kohn–Sham (KS) orbitals, optimized for the dominant closed-shell determinant of the electronic ground state employing the BH-LYP functional.[18,19] All valence electrons were correlated in the MRCI runs. The lowest five roots in the singlet manifold were calculated. The initial set of CSFs was generated from all single and double excitations out of the five highest occupied molecular orbitals in the KS determinant into the five lowest virtual orbitals and was then iteratively improved. The size of the MRCI expansion was kept moderate by selection of the most important configurations, based on an energy gap criterion,[17] leading to 31399 configurations with which the calculations where performed.

Additionally, a natural bond orbital analysis using the NBO 3.1 program,[20] implemented in the Gaussian 03 program package (Revision C.02)[21] was performed using the wavefunctions from a (TD) B3LYP-optimized structure using Dunnings cc-pVTZ basis set.

2.2. Evolution Strategies

The rovibronic spectra were fit to an asymmetric rotor Hamiltonian[22] by using the de-randomized (DR) evolution strategy (ES) developed by Ostenmeier et al.[23] A special implementation which we have employed herein represents the second generation of de-randomized ES, abbreviated as DR2.[24] It was recently shown[25] to be a very good alternative to the genetic algorithm-based fits we have employed so far.[26] Evolutionary strategies such as the DR2 algorithm are global optimizers which are inspired by the biological processes of reproduction and natural selection. While classical genetic algorithms aim to find a solution in the parameter space by randomly combining information from a set of trial solutions, the DR2 algorithm can sense in which direction the goodness of the fit (the so-called cost function) increases. In the first step, the DR2 algorithm generates trial solutions (offspring) by using a random distribution around some starting point (parent), each consisting of the complete parameter set which is necessary to simulate the spectrum. Offspring with higher fitness than the parent are kept and used to compute the next generation. The DR2 algorithm makes use of the parameter correlation matrix for successive changes in the parents (mutations). This means that if for some parameter a parent has evolved in the same direction for several generations, resulting in a positive correlation, the most likely solution is assumed to be further in that direction and the next parameter mutation will be larger. Correspondingly, two anticorrelated mutations will lead to a smaller mutation. Compared to classical genetic algorithms, this procedure has been shown to lead to a faster convergence of the parameters.[25]

Experimental Section

1,4-Benzodioxan (purity $>97\,\%$) was purchased from Sigma Aldrich and used without further purification.

The experimental setup for the rotationally resolved laser-induced fluorescence is described in detail elsewhere.[27] Briefly, the laser system consisted of a single-frequency ring dye laser (Sirah Matisse DS) operated with Rhodamine 110, pumped with 7 W of a frequency-doubled continuous wave (cw) Nd:YAG laser (Spectra Physics, Millenium X). The dye laser output was coupled to an external folded ring cavity (Spectra Physics Wavetrain) for second-harmonic generation. The resulting output power was constant at about 25 mW during each experiment. The molecular beam was formed by co-expanding 1,4-benzodioxan heated to 120 °C and Ar as carrier gas through a 200 μm nozzle into the vacuum. The molecular beam machine consisted of three differentially pumped vacuum chambers that were linearly connected by skimmers (1 mm and 3 mm, respectively) to reduce the Doppler width to 18 MHz in this setup (full-width-at-half-maximum, FWHM). In the third chamber, 360 mm downstream of the nozzle, the molecular beam crossed the laser beam at a right angle. The imaging optics setup consistd of a concave mirror and two plano-convex lenses to collect the resulting fluorescence onto a photomultiplier tube which was mounted perpendicular to the plane defined by the laser and the molecular beam. The signal output was then discriminated and digitized by a photon counter and transmitted to a PC for data recording and processing. The relative frequency was determined with a quasi-confocal Fabry-Perot interferometer with a free spectral range (FSR) of 149,9434(56) MHz. The absolute frequency was obtained by comparing the recorded iodine absorption spectrum with tabulated lines.

3. Results and Discussion

3.1. Quantum Chemical Calculations

3.1.1. The Electronic Ground State

We calculated three structures with different symmetries [planar (C_{2v}), boat (C_s), and twist (C_2)], which can be assumed to be the minimum structure using CC2-coupled cluster theory with the correlation consistent cc-pVTZ basis set. Table 1 compares the structural parameters (rotational constants and inertial defect) and the relative energies of the three structures. The inertial defect is defined as $\Delta I = I_c - I_a - I_b$, where the I_g are the moments of inertia about the principal inertial axes g. For a planar molecule, it is zero and negative for nonplanar molecules. Vibrational effects actually cause the inertial defects of perfectly planar molecules to deviate slightly from zero. ΔI thus provides a measure for the non-planarity of a molecule.

Table 1. CC2/cc-pVTZ-calculated relative energies, rotational constants (*A*,*B*,*C*), inertial defects (ΔI), and center frequency of absorption (ν_0) of three different stationary points on the potential energy surface of 1,4-benzodioxan in their electronic ground (doubly primed quantities) and first excited (primed quantities) singlet state.

	Twisted (C_2)	Boat (C_s)	Planar (C_{2v})
E_{rel} [cm^{-1}]	0	2837	4085
A'' [MHz]	2914.9	2859.7	2893.6
B'' [MHz]	1237.8	1241.4	1206.7
C'' [MHz]	892.2	904.8	860.7
$\Delta I''$ [uA^2]	−15.22	−25.28	−6.29
ν_0 [cm^{-1}]	36114	36083	35785
A' [MHz]	2815.5	2836.6	2795.0
B' [MHz]	1232.1	1216.9	1204.0
C' [MHz]	881.3	872.2	850.4
$\Delta I'$ [uA^2]	−16.20	−14.03	−6.27
ΔA [MHz]	−99.4	−23.1	−98.6
ΔB [MHz]	−5.7	−24.5	−2.7
ΔC [MHz]	−10.9	−32.6	−10.3

All three structures exhibit sufficiently different rotational constants to make a straightforward assignment to the experimentally observed form, from a comparison to the experimental rotational constants. Especially the inertial defects ΔI, which give a direct measure for the degree of non-planarity, make the assignment to the twist form straightforward.

The three structures are shown in Figure 1. The lowest energy structure is the twist form. The boat form is higher in energy, by 2837 cm^{-1}, and the planar BZD by 4085 cm^{-1}. The boat form is a first-order saddle point connecting the two enantiomeric twist forms. The planar form represents a second-order saddle point connecting two identical boat forms via the first motion with imaginary frequency and two identical twist forms via the second motion with imaginary frequency.

A comparison of the rotational constants and the inertial defects with the experimental values from Table 3 immediately shows that the twisted structure is responsible for all the features observed in the fluorescence spectra. Also, the changes in the rotational constants upon electronic excitation are in very good agreement with the experimentally determined values for the twisted form.

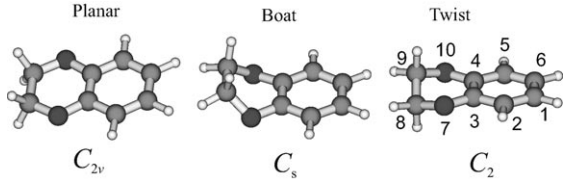

Figure 1. Structures of the three lowest energy structures of BZD: planar (C_{2v}), boat (C_s), and twisted (C_2), along with the atomic numbering.

3.1.2. The Lowest Excited Singlet States

The structures of the two lowest excited singlet states of the twisted, boat, and planar forms of BZD were optimized at the CC2/cc-pVTZ level of theory. The barrier for interconversion of the two enantiomeric twisted forms over the boat transition state amounts to 3930 cm^{-1}, slightly lower than in the electronic ground state. The difference to the second-order transitions state (the planar form) is calculated to be 2768 cm^{-1}, also slightly lower than the value for the S_0 state.

Vertical and adiabatic excitation energies and transition dipole moments of the lowest four electronic singlet states of BZD were calculated at the CC2 level and using DFT/MRCI. The results are compiled in Table 2. The lowest electronically excited singlet state is polarized along the long (*a*) inertial axis and must therefore be classified as ^1L_b state in the nomenclature of Platt.[28] The excitation is mainly from HOMO to LUMO (17b–18b) and to a lesser extent from HOMO-1 to LUMO + 1 (19a–20a), see Figure 2. The second excited singlet state is polarized along the *b* axis and therefore represents the ^1L_a state. It is mainly a HOMO–LUMO + 1 excitation (17b–20a).Two more ex-

Table 2. Calculated vertical and adiabatic singlet excitation energies ΔE [cm^{-1}] and transition dipole moment orientations of BZD. The parameter θ describes the in-plane angle of the TDM with the inertial *a* axis. All the adiabatic excitation energies are zero-point-energy-corrected at the CC2/cc-pVTZ level of theory.

	$L_b \leftarrow S_0$		θ	$L_a \leftarrow S_0$		θ	$B_b \leftarrow S_0$		θ	$B_a \leftarrow S_0$		θ
	vert.	adiab.		vert.	adiab.		vert.	adiab.		vert.	adiab.	
CC2	38975	36114	0	47108	43339	90	52705	48149	90	52541	49884	0
DFT/MRCI	38245	36050	0	47300	44441	90	53237	50055	90	53369	48880	0
Exp.		35560	6									

Table 3. Molecular constants of the origin and three vibration bands of 1,4-benzodioxan obtained from ES-DR2 fits to the experimental spectra.

	Origin	25_0^1	48_0^2	18_0^1
A'' [MHz]	2920.0(4)	2920.1(1)	2919.8(5)	2919.3(3)
B' [MHz]	1235.22(1)	1235.26(2)	1235.43(3)	1235.34(4)
C' [MHz]	891.05(1)	891.04(1)	891.08(2)	891.21(2)
$\Delta I''$ [uA^2]	−15.0405	−15.0524	−14.8993	−15.1338
ΔA [MHz]	−92.81(1)	−92.82(1)	−102.04(1)	−93.06(2)
ΔB [MHz]	−6.69(1)	−6.71(1)	−3.35(1)	−7.01(2)
ΔC [MHz]	−9.68(1)	−9.68(1)	−7.14(1)	−9.15(2)
$\Delta I'$ [uA^2]	−16.7226	−16.7362	−17.7377	−17.2907
θ [degree]	6(1)	18(1)	19(1)	2(2)
ϕ [degree]	87(1)	86(1)	87(1)	86(2)
τ [ns]	6.2(1)	6.8(1)	6.3(1)	6.2(1)
T_1	1.55	1.85	1.50	1.50
T_2	2.95	3.45	4.96	2.77
w	0.3	0.12	0.13	0.17
μ_a	0.98	0.98	0.92	1.00
μ_b	0.02	0.02	0.08	0.00
μ_c	0.00	0.00	0.00	0.00
ν_0 [cm^{-1}]	35560.15(2)	35699.33(2)	35718.72(2)	36262.06(2)
$\Delta\nu$ [cm^{-1}]	0	139.18(2)	158.57(2)	701.91(2)

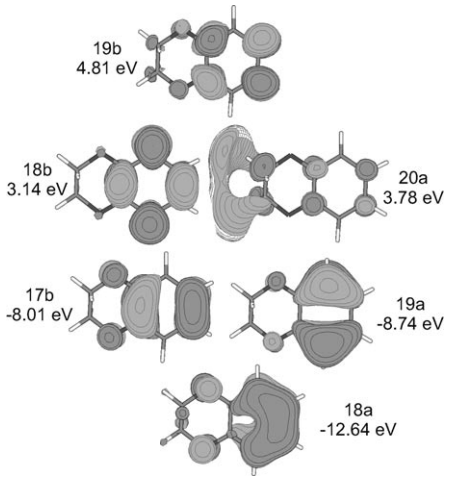

Figure 2. Frontier orbitals of the twisted form of BZD at the CC2/cc-pVTZ level of theory.

cited singlet states have been calculated, namely, the ^1B_a and the ^1B_b states. The first of these is classified as HOMO-2 to LUMO+1 (18a-20a), the next as HOMO to LUMO+1 (17b–20a). The purely electronic ^1B_a and ^1B_b states are quasi-degenerate at the DFT/MRCI level of theory; inclusion of zero-point energy brings the ^1B_a state slightly below the ^1B_b state. Oscillator strengths (*f*) of 0.0207, 0.0023, 0.7571, and 0.4743 are found for the ^1L_b, ^1L_a, ^1B_b, and ^1B_a states, respectively.

Regarding the large energy gap of more than 8000 cm^{-1} between the ^1L_b and the ^1L_a state and the small oscillator strength of the latter, no vibronic coupling between vibronic bands of the ^1L_b state and the origin of the ^1L_a state is expected.

3.2. The vibrational and Vibronic Spectrum of BZD

The vibrational and vibronic spectra of the twisted form of BZD were calculated at the CC2/cc-pVTZ level of theory. Twenty-five of the 48 vibrations in the C_2 point group transform like the totally symmetric representation *a*, and 23 vibrations like the nontotally symmetric representation *b*. The lowest electronically excited state has its transition dipole moment oriented along the molecular *a* axis. The transition dipole moment transforms like *A* along the inertial *a* axis and like *B* along the *b* and *c* axes. The pure electronic ($\pi\pi^*$) transition is therefore classified as $A \leftarrow A$. Thus, the totally symmetric vibrational (and vibronic) bands will exhibit *A*-type selections rules, while the nontotally symmetric vibrations will be *BC* hybrid bands.

The calculated ground-state vibrations are given by ascending frequencies in Table S1 of the Supporting Information. The calculated frequencies are compared to experimental vibrational frequencies from ref. [11]. The following columns give the calculated and experimental vibrational frequencies in the first electronically excited state of *A* symmetry. In order to make the assignment of excited-state to ground-state vibrations, we calculated the Duchinsky matrix from the hessians of both electronic states. The normal coordinates Q' of the excited state and Q'' of the ground state are related by the linear orthogonal transformation given by Duchinsky [Eq. (1)]:[29]

$$\mathbf{Q}'' = \mathbf{S}\mathbf{Q}' + \vec{d} \quad (1)$$

where $\vec{d}$ is a displacement vector and **S** is the Duchinsky matrix, which rotates the coordinate system of one state into that of the other state. The largest elements of the complete Duchinsky matrix is given in the last column in Table S1 of the Supporting Information. The lowest nontotally symmetric vibrations Q_{48} and Q_{47} are strongly Duschinsky-mixed, with nearly equal coefficients for both vibrations. This behavior has been inferred by Gordon and Hollas[3] from the massive occurrence of cross-sequences of the form $48_0^x 47_x^0$. While in the low-frequency region strong Duchinsky mixing is found, there is only very little mixing above 500 cm^{-1} and the vibrations retain their identities upon electronic excitation.

3.3. Rotationally Resolved Electronic Spectra

3.3.1. The Electronic Origin

We measured the rotationally resolved electronic spectrum of the electronic origin of BZD in a molecular beam (cf. Figure 3). For the simulation of the rovibronic spectra a rigid asymmetric

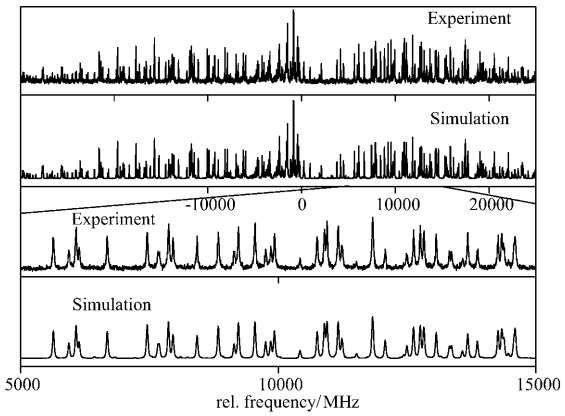

Figure 3. Rotationally resolved electronic spectrum of the electronic origin of BZD. The second trace shows the simulation using the best parameters from Table 3. The lowest traces show zoomed-in parts of the experimental spectrum and the simulation.

rotor Hamiltonian was employed.[22] The origin spectrum was fitted to the rotational constants *A*, *B*, and *C* in both electronic states, to the center frequency ν_0, to the orientation of the transition dipole moment with respect to the inertial axes measured by the polar angles θ and ϕ, the rotational temperature in the jet and a Lorentz and Doppler width, for the lineshape profile using an evolutionary strategy approach. The temperature dependence of the intensity is described by a two-temperature model [Eq. (2)]:

$$n(E, T_1, T_2, w) = e^{-E/kT_1} + we^{-E/kT_2} \quad (2)$$

where E is the energy of the lower state, k is the Boltzmann constant, w is a weighting factor, T_1 and T_2 are the two temperatures.[30] For details of the evolution strategy see Section 2.2.

The molecular parameters from the fit are collected in Table 3. A comparison of the rotational constants and inertial defects of the three BZD structures from Table 1 with the experimental values immediately shows that the observed spectrum is due to the twisted form.

The electronic transition moment is oriented along the (long) inertial a axis. According to Platt's nomenclature, this is the signature of the ^1L_b state, which has the transition moment vector running through the **b**onds, while that of the ^1L_a state runs through the **a**toms.

The change of the inertial defect from -15.04 to -16.72 uA^2 shows that the BZD molecule gets considerably more nonplanar upon electronic excitation. This is exactly the trend which is obtained from the CC2 calculations described in Section 3.1 for the twisted from (increase of ΔI from -15.22 to -16.20 uA^2). Also, the structurally similar 1,3-benzodioxole (BDO), which has been recently investigated in the Pratt[31] and the Laane groups,[8] shows a larger inertial defect in the electronically excited state. There, the increasing non-planarity was attributed to the ability of the p-type lone pair (LP) at the oxygen atom to either conjugate with the π electrons of the benzene ring or interact with the σ^* orbital of the adjacent CO and the axial CH bonds. This inverse hyperconjugation (the anomeric effect) is strongly stabilizing and leads to a puckering of the five-membered ring. In the excited state, the weaker interaction of the LP with the aromatic ring leads to an increased anomeric effect and to a stronger non-planarity of the system as has been discussed by Thomas et al.[31]

For BZD, the only possible anomeric interaction is between the oxygen lone pairs (donor) and the the σ^* orbitals of the adjacent axial CH bonds (acceptor). The importance of the stabilizing anomeric effect in this molecule can be established from the ab initio calculations in various ways: First, from the CC2 calculations we learn that the C–H bond lengths of the axial H atoms of the bridging CH_2 groups are larger than the equatorial ones (1.0936 Å vs. 1.0878 Å) as a consequence of the $\pi(O_{LP})\rightarrow\sigma^*(C\text{–}H_{ax})$ interaction. Secondly, an NBO analysis using the B3-LYP/cc-pVTZ-optimized structure shows a larger Wiberg bond order between the oxygen atom and the axial H atom (0.0215) compared to the equatorial H atom (0.0041). The stabilization energy from a charge transfer from the oxygen LP with 100% p-character to the σ^* CH bond $[0.6(sp^3)_C\text{-}0.8(s)_H)]$ amounts to 29.6 kJ mole^{-1}. Figure 4 shows the two natural bond orbitals that are responsible for the interaction which stabilizes the puckered form. On the left-hand side of Figure 4, the p-type oxygen lone pair is shown and on the right-hand side the antibonding σ^* orbital of the adjacent CH_2 group as obtained from the NBO analysis.

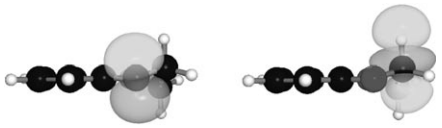

Figure 4. Side view of the p-type oxygen lone pair (left) and the antibonding σ^* orbital of the adjacent ĐCH$_2$Đ group (right) in ground-state BZD.

Upon electronic excitation, the electron density is shifted from the oxygen lone pair to the aromatic ring, such as in the case of phenol[33] (cf. also Figure 2). This effect is also quantified through the ab initio calculations: The Wiberg bond order (NBO) index between the oxygen atom and the axial H atom decreases upon electronic excitation from 0.0215 to 0.0204, while the bond order between the oxygen and the adjacent ring carbon atom increases from 0.9781 to 0.9871. The charge-transfer stabilization from the oxygen lone pair to the antibonding σ^* CH bond is smaller (28.4 kJ mole^{-1}) than in the electronic ground state. Thus, it can be inferred from the calculations that the explication given in refs. [8,31] for the increased non-planarity upon electronic excitation in BDO does not apply for BZD.

Comparison of the ground- and excited-state structures of BZD reveals an important detail: While the O atoms in ground-state BZD are situated in the plane of the aromatic ring (upper trace in Figure 5), they are slightly out-of-plane in the excited state. The $O_7O_{10}C_4C_3$ dihedral angle from the CC2 calculations is 0.5° in the ground state and 5° in the excited state. The lower two traces of Figure 5 give two different side views of excited-state BZD: the first projection shows that one of the O atoms is located above the aromatic ring, the other below. The second projection places the two O atoms in the line of view. In this perspective, it can be seen that the heterocyclic six-ring adopts a half-chair configuration as found for the non-aromatic analogue 2,3-dihydro-1,4-dioxin.[32] Since electronic excitation reduces the bond orders in the aromatic ring due to the $\pi\pi^*$ excitation, the forced co-planarity of the aromatic ring and the oxygen atoms in the electronic ground state is released in favor of the sterically more stable nonplanar form.

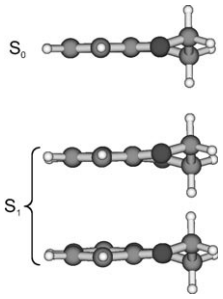

Figure 5. Side view of the ground-state structure (upper trace) and of two different side views of the lowest excited singlet state.

3.3.2. Higher Vibronic Bands

Figure 6 shows the rotationally resolved spectrum of the A vibration Q_{25} at 0,0 + 139 cm^{-1}. The parameters from the best fit are compiled in Table 3. The band is a pure a-type band, such as the electronic origin. This is what can be expected for the vibrations with A-symmetry. The change of the inertial defect upon electronic excitation nearly matches the one of the elec-

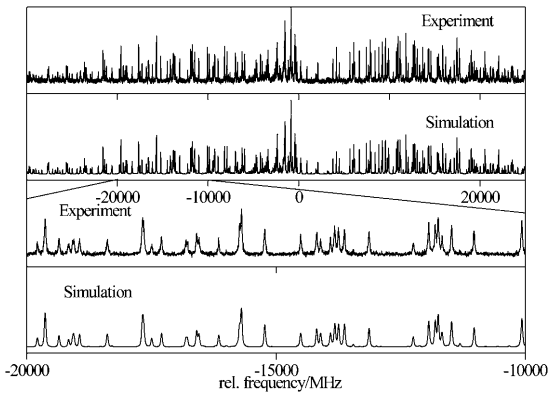

Figure 6. Rotationally resolved electronic spectrum of the 139 cm^{-1} band of BZD. The second trace shows the simulation using the best parameters from Table 3. The lowest traces show zoomed-in parts of the experimental spectrum and the simulation.

tronic origin, thus giving further evidence for the assignment of this band as being of *A* symmetry.

Figure S1 of the Supporting Information shows the rotationally resolved spectrum of the first overtone of the *B* vibration Q_{48} at $0,0+159\ cm^{-1}$. The parameters from the best fit are also compiled in Table 3. The overtone of this *B* vibration is also of *A* symmetry as the electronic origin, and shows consequently an *a*-type contour. For this band a considerably larger change of the inertial defect upon electronic excitation is found than for the origin and the $0,0+139\ cm^{-1}$ bands.

The rotationally resolved spectrum of the *A* vibration Q_{18} at $0,0+702\ cm^{-1}$ is shown in Figure S2 of the Supporting Information. The parameters from the best fit are compiled in Table 3. This band was previously assigned as Q_{21}. As a result of our normal-mode and Duchinsky analysis we reassign this band as being due to Q_{18}.

The excited-state lifetimes of the electronic origin and of all the vibronic bands investigated herein were determined from the Lorentz contribution of the Voigt profiles of the rovibronic lines. They are remarkably similar, around 6.5 ns.

4. Conclusions

The rotationally resolved electronic spectra of BZD have shown that this molecule exists in the twisted form in both electronic states. The main factor for the stabilization of the twisted form is the steric repulsion of the adjacent CH_2 groups. The non-planarity of BZD in both states has been measured through the inertial defect. It is shown that BZD is more planar in the electronic ground state than in the electronically excited state. The reason for the larger non-planarity of the system is the reduced C–C bond order in the aromatic ring upon electronic $\pi\pi^*$ excitation. The O atoms, whose *p*-type lone pairs can be partially delocalized into the aromatic ring, adopt a structure with less steric strain in the excited state and therefore leave the aromatic plane, thereby leading to a larger inertial defect.

Supporting Information Available: The rovibronic spectra at $0,0+139\ cm^{-1}$ and $0,0+702\ cm^{-1}$ are available as Supporting Information.

Acknowledgements

This work was supported by the Netherlands Organization for Scientific Research (NWO), and the Deutsche Forschungsgemeinschaft in the framework of the NWO-DFG bilateral program Grant No. SCHM1043/10 (Germany) and DN 72-248 (The Netherlands).The authors would like to thank the National Computer Facilities of the Netherlands Organization of Scientific Research (NWO) for a grant on the Dutch supercomputing facility SARA. Granted computing time at Universitätsrechenzentrum Köln is gratefully acknowledged.

Keywords: ab initio calculations · anomeric effect · ring puckering · rovibronic · spectroscopy

[1] R. D. Gordon, J. M. Hollas, *J. Mol. Spectrosc.* **1992**, *156*, 415 – 420.
[2] R. D. Gordon, J. M. Hollas, *J. Mol. Struct.* **1993**, *293*, 193 – 196.
[3] R. D. Gordon, J. M. Hollas, *J. Chem. Phys.* **1993**, *99*, 3380 – 3389.
[4] R. D. Gordon, J. M. Hollas, *J. Mol. Spectrosc.* **1994**, *163*, 159 – 179.
[5] J. Yang, M. Wagner, J. Laane, *J. Phys. Chem. A* **2007**, *110*, 9805 – 9815.
[6] J. Yang, J. Choob, O. Kwon, J. Laane, *Spectrochim. Acta Part A* **2007**, *68*, 1170 – 1173.
[7] J. Yang, J. Laane, *J. Mol. Struct.* **2006**, *798*, 27 – 33.
[8] J. Laane, E. Bondoc, S. Sakurai, K. Morris, N. Meinander, J. Cho, *J. Am. Chem. Soc.* **2000**, *122*, 2628.
[9] S. Moon, Y. Kwon, J. Lee, J. Choo, *J. Phys. Chem. A* **2001**, *105*, 3221 – 3225.
[10] D. Suárez, T. L. Sordo, J. A. Sordo, *J. Am. Chem. Soc.* **1996**, *118*, 9850 – 9854.
[11] J. Choo, S. Yoo, S. Moon, Y. Kwon, H. Chung, *Vib. Spectrosc.* **1998**, *17*, 173 – 182.
[12] R. Ahlrichs, M. Bär, M. Häser, H. Horn, C. Kölmel, *Chem. Phys. Lett.* **1989**, *162*, 165 – 169.
[13] A. Schäfer, C. Huber, R. Ahlrichs, *J. Chem. Phys.* **1994**, *100*, 5829 – 5835.
[14] C. Hättig, F. Weigend, *J. Chem. Phys.* **2000**, *113*, 5154 – 5161.
[15] C. Hättig, A. Köhn, *J. Chem. Phys.* **2002**, *117*, 6939 – 6951.
[16] C. Hättig, *J. Chem. Phys.* **2002**, *118*, 7751 – 7761.
[17] S. Grimme, M. Waletzke, *J. Chem. Phys.* **1999**, *111*, 5645 – 5655.
[18] A. D. Becke, *J. Chem. Phys.* **1993**, *98*, 1372 – 1377.
[19] C. Lee, W. Yang, R. Parr, *Phys. Rev. B* **1988**, *37*, 785 – 789.
[20] E. D. Glendening, A. E. Reed, J. E. Carpenter, F. Weinhold, *NBO Version 3.1*, Madison.
[21] *Gaussian 03* (Revision C.02), M. J. Frisch, G. W. Trucks, H. B. Schlegel, G. E. Scuseria, M. A. Robb, J. R. Cheeseman, J. A. Montgomery, Jr., T. Vreven, K. N. Kudin, J. C. Burant, J. M. Millam, S. S. Iyengar, J. Tomasi, V. Barone, B. Mennucci, M. Cossi, G. Scalmani, N. Rega, G. A. Petersson, H. Nakatsuji, M. Hada, M. Ehara, K. Toyota, R. Fukuda, J. Hasegawa, M. Ishida, T. Nakajima, Y. Honda, O. Kitao, H. Nakai, M. Klene, X. Li, J. E. Knox, H. P. Hratchian, J. B. Cross, V. Bakken, C. Adamo, J. Jaramillo, R. Gomperts, R. E. Stratmann, O. Yazyev, A. J. Austin, R. Cammi, C. Pomelli, J. W. Ochterski, P. Y. Ayala, K. Morokuma, G. A. Voth, P. Salvador, J. J. Dannenberg, V. G. Zakrzewski, S. Dapprich, A. D. Daniels, M. C. Strain, O. Farkas, D. K. Malick, A. D. Rabuck, K. Raghavachari, J. B. Foresman, J. V. Ortiz, Q. Cui, A. G. Baboul, S. Clifford, J. Cioslowski, B. B. Stefanov, G. Liu, A. Liashenko, P. Piskorz, I. Komaromi, R. L. Martin, D. J. Fox, T. Keith, M. A. Al-Laham, C. Y. Peng, A. Nanayakkara, M. Challacombe, P. M. W. Gill, B. Johnson, W. Chen, M. W. Wong, C. Gonzalez, J. A. Pople, Gaussian, Inc., Wallingford, CT, **2004**.
[22] H. C. Allen, P. C. Cross, *Molecular Vib-Rotors*, Wiley, New York, **1963**.
[23] "Step-Size Adaptation Based on Non-Local Use of Selection Information": A. Ostermeier, A. Gawelczyk, N. Hansen in *Lecture Notes in Com-*

puter Science: Parallel Problem Solving from Nature (PPSN III) (Eds.: Y. Davidor, H.-P. Schwefel, R. Männer), Springer, Heidelberg, **1994**.
[24] "The Second Harmonic Generation Case Study as a Gateway for ES to Quantum Control Problems": O. M. Shir, T. Bäck in *Proceedings of the Genetic and Evolutionary Computation Conference*, ACM Press, London, **2007**.
[25] I. Kalkman, C. Vu, M. Schmitt, W. L. Meerts, *ChemPhysChem* **2008**, *9*, 1788 – 1797.
[26] W. L. Meerts, M. Schmitt, *Int. Rev. Phys. Chem.* **2006**, *25*, 353 – 406.
[27] M. Schmitt, J. Küpper, D. Spangenberg, A. Westphal, *Chem. Phys.* **2000**, *254*, 349 – 361.
[28] J. R. Platt, *J. Chem. Phys.* **1949**, *17*, 484 – 495.
[29] F. Duschinsky, *Acta Physicochim. URSS* **1937**, *7*, 551 – 577.
[30] Y. R. Wu, D. H. Levy, *J. Chem. Phys.* **1989**, *91*, 5278 – 5284.
[31] J. A. Thomas, L. Alvarez-Valtierra, D. W. Pratt, *Chem. Phys. Lett.* **2010**, *490*, 109 – 115.
[32] F. Freeman, C. Lee, W. J. Hehre, H. N. Po, *J. Comput. Chem.* **1997**, *18*, 1392 – 1406.
[33] C. Ratzer, J. Küpper, D. Spangenberg, M. Schmitt, *Chem. Phys.* **2002**, *283*, 153 – 169.
[34] M. A. R. Matos, C. C. S. Sousa, V. M. F. Morais, *J. Phys. Chem. A* **2008**, *112*, 7961 – 7968.

Received: July 16, 2010
Revised: October 6, 2010
Published online on January 14, 2011

